J Appl Physiol 131: 1708–1717, 2021.
First published October 14, 2021; doi:10.1152/japplphysiol.01119.2020

american physiological society

JOURNAL OF APPLIED PHYSIOLOGY

RESEARCH ARTICLE

Supraspinatus muscle architecture and physiology in a rabbit model of tenotomy and repair

Sydnee A. Hyman,[1,2] Isabella T. Wu,[2] Laura S. Vasquez-Bolanos,[1,2] Mackenzie B. Norman,[2,3] Mary C. Esparza,[2] Shannon N. Bremner,[2] Shanelle N. Dorn,[2] Ivan Ramirez,[2] Donald C. Fithian,[2] John G. Lane,[2] Anshuman Singh,[2,4] and Samuel R. Ward[1,2,5]

[1]*Department of Bioengineering, University of California, San Diego, California;* [2]*Department of Orthopaedic Surgery, University of California, San Diego, California;* [3]*Dartmouth Geisel School of Medicine, Hanover, New Hampshire;* [4]*Department of Orthopaedic Surgery, Kaiser Permanente, San Diego, California; and* [5]*Department of Radiology, University of California, San Diego, California*

Abstract

Chronic rotator cuff tears can cause severe functional deficits. Addressing the chronic fatty and fibrotic muscle changes is of high clinical interest; however, the architectural and physiological consequences of chronic tear and repair are poorly characterized. We present a detailed architectural and physiological analysis of chronic tear and repair (both over 8 and 16 wk) compared with age-matched control rabbit supraspinatus (SSP) muscles. Using female New Zealand White Rabbits (n = 30, n = 6/group) under 2% isoflurane anesthesia, the SSP was surgically isolated and maximum isometric force was measured at four to six muscle lengths. Architectural analysis was performed, and maximum isometric stress was computed. Whole muscle length-tension curves were generated using architectural measurements to compare experimental physiology to theoretical predictions. Architectural measures are consistent with persistent radial and longitudinal atrophy over time in tenotomy that fails to recover after repair. Maximum isometric force was significantly decreased after 16 wk tenotomy and not significantly improved after repair. Peak isometric force reported here are greater than prior reports of rabbit SSP force after tenotomy. Peak stress was not significantly different between groups and consistent with prior literature of SSP stress. Muscle strain during contraction was significantly decreased after 8 wk of tenotomy and repair, indicating effects of tear and repair on muscle function. The experimental length-tension data were overlaid with predicted curves for each experimental group (generated from structural data), exposing the altered structure-function relationship for tenotomy and repair over time. Data presented here contribute to understanding the physiological implications of disease and repair in the rotator cuff.

NEW & NOTEWORTHY We utilize an established method to measure the length-tension relationship for the rabbit supraspinatus in normal, torn, and repaired muscles. We then perform architectural analysis to evaluate structural changes after tear and repair. Although peak isometric force is lower in the tear and repair groups, there are no differences in peak stresses across groups. These findings indicate persistent structural changes (both radial and longitudinal atrophy) and physiological deficiencies (decreased peak force and uncoupling structure-function relationship) after tenotomy that do not significantly recover after repair.

architecture; muscle force; muscle physiology; muscle stress; rotator cuff

INTRODUCTION

Chronic rotator cuff (RC) tendon tears cause progressively decreased muscle quality (atrophy, fatty infiltration, and fibrosis) that persists despite clinically successful repair (1, 2). These changes to the muscles are not only painful and functionally devastating to the patient but are also predictive of negative surgical outcomes (3–7). Although the focus of some contemporary research has been on halting or reversing the fibrosis, fatty infiltration, and atrophy (8–10), little attention has been paid to addressing the profound architectural changes to chronically torn RC muscles (11, 12). Both decreased muscle quality and changes in muscle architecture are likely to affect muscle function, yet the physiological consequences of these muscular changes after RC tear and repair are largely unknown. One study measured supraspinatus (SSP) contractile muscle force intraoperatively in human (13), one group reported infraspinatus contractile force in sheep (3, 14), and two groups reported SSP contractile force in rabbit (15, 16) after tenotomy. Of these studies, none has measured contractile force after repair.

Correspondence: S. R. Ward (s1ward@ucsd.edu).
Submitted 5 January 2021 / Revised 20 September 2021 / Accepted 11 October 2021

Although decreased muscle cross-sectional area (CSA) has a clear link to decreased peak muscle force (13, 14, 16, 17), there are a number of cellular and structural changes in torn RC muscles that could impact muscle physiology (11, 18–20). For example, a recent study in rabbit claimed that fatty infiltration was a better predictor of muscle weakness than atrophy (16). However, a variety of structural changes may impact function: shorter muscles and fiber lengths may indicate serial sarcomere loss (11, 12) (which may impair muscle operating range); increased pennation angles may be a compensatory mechanism to retain some force production after tear (21–23); and secondary muscle injury from repair may result in both loss of E-C coupling and more fibrosis (18), further impairing force production (11, 24). However, no in-depth evaluation of the architectural changes that occur after tear and repair has been performed in an animal model.

Therefore, the objective of this study is to measure the architectural changes and physiological consequences of rotator cuff tenotomy and repair. To reasonably recapitulate several important clinical characteristics of RC tear (muscle retraction, muscle atrophy, fatty infiltration, and inflammation), we used a rabbit model (9, 25–28). We hypothesize that architectural features will demonstrate radial and longitudinal atrophy, tenotomy and repair will cause more strain during contraction, and muscle function will be impaired (measured by peak isometric force and narrow length-tension curves). This should enable researchers assessing RC tear pathology to benchmark functional outcomes and test the functional consequences of novel therapies.

MATERIALS AND METHODS

Animals

All experimental procedures were approved by the Institutional Animal Care and Use Committee (IACUC) of the University of California, San Diego. Thirty skeletally mature female New Zealand White Rabbits (n = 6/group) were used for this study. The animals used for intervention groups (both 8 and 16 wk tenotomy, and 8 and 16 wk repair) were 6-mo old at the beginning of the study. To account for animal growth over the course of the study, control rabbits were age-matched to the final age of the intervention group rabbits, roughly 1-yr old. Mean body weight at euthanasia was 4.36 kg, 4.05 kg, 4.30 kg, 4.57 kg, and 4.24 kg for the age-matched control, 8 wk tenotomy, 16 wk tenotomy, 8 wk repair, and 16 wk repair groups, respectively.

Cage locations were assigned upon arrival, each rabbit was given a number ID, and then randomized to one of the study groups. Researchers were aware of the allocation during the surgeries and tissue harvest, but the specimens were identified by ID number only. Animals were single-housed with food and water ad libitum, environmental and food enrichment, and visual access to other animals. There were no adverse events in this study and no animals met the criteria for humane endpoints. These criteria included: displaying clinical signs of disease, loss of appetite, weight below 15% of what is expected for the animal, and/or signs of distress, such as self-mutilation.

Surgical Procedures

For all surgical procedures, rabbits were anesthetized with a subcutaneous injection of a ketamine-xylazine cocktail (50 and 5 mg/kg body mass, respectively) and maintained on 2% isoflurane anesthesia. Heart rate and oxygen saturation were monitored (VetOx, Heska Co., Fort Collins, CO) throughout the test duration. The left supraspinatus (SSP) muscle served as the experimental side in all animals, with the contralateral shoulder as an unoperated internal control.

All intervention groups underwent the following tenotomy procedure (Fig. 1). An open anterior approach was performed on the left shoulder, followed by sharp transection of the left SSP tendon from its footprint on the greater tuberosity of the humerus. The surrounding soft tissues were bluntly dissected to allow unhindered retraction of the tendon stump and distal muscle. After securing a Penrose drain to the tendon stump to prevent scar formation between the tendon and surrounding soft tissue, the incision was closed in layers.

Rabbits were then allowed individual cage activity with routine postoperative care. Buprenorphine SR (0.1 mg/kg) was used for analgesia, and the animals were monitored daily for 2 wk postoperatively.

The two repair groups underwent a SSP repair procedure 8 wk after tenotomy. Using the same anesthesia and anterior approach as the tenotomy, the repair was performed using a modified locking suture with anterior and posterior bone tunnels to restore the tendon footprint to the humeral head. Fibrous adhesions and any remaining tendon stump on the greater tubercle of the humerus were debrided to allow for tendon-to-bone healing after SSP repair. Closure and postoperative protocols were the same as above.

All animals underwent the following procedure to test the length-tension relationship in the SSP using methods previously described (29). Briefly, under anesthesia, an open approach was used to expose the SSP by dividing the middle trapezius and deltoid muscles. The suprascapular nerve was isolated by blunt dissection around the anterior aspect of the SSP (30), and a cuff electrode (Pulsar 6Bp Stimulator; FHC, Bowdoinham, ME) was placed around the nerve for direct stimulation. Nerve isolation was confirmed by delivering twitch stimulations and visualizing supraspinatus contraction. The distal SSP tendon was transected, released from the superior joint capsule, sutured to a servomotor (Cambridge Model 310B; Aurora Scientific, Aurora, ON, Canada), and aligned with the force-generating axis of the motor. Care was taken to securely suture the tendon, which is particularly important after a period of tenotomy where the tendon degenerates to some degree. Here, two suture techniques were used simultaneously to prevent suture slippage and tendon rupture (2-0 FiberWire, Arthrex, Naples, FL): an infinity stitch and a modified Kessler stitch, both of which are designed to prevent shearing of the suture through the tendon fibers and tighten under load. Each tendon (in all groups) was sutured through the external (bare) tendon and through the distal aponeurotic attachment, and this set of locking sutures was monitored during testing through video-based strain measurements and careful examination of each force record. Muscle temperature was maintained at 37°C with radiant heat, heated saline, and a servo-temperature controller (Model 73 A; YSI, Yellow Springs, OH). A custom-built clamp was used to immobilize the scapula, placed from the vertebral border along the scapular spine and bolted through the infraspinous fossa.

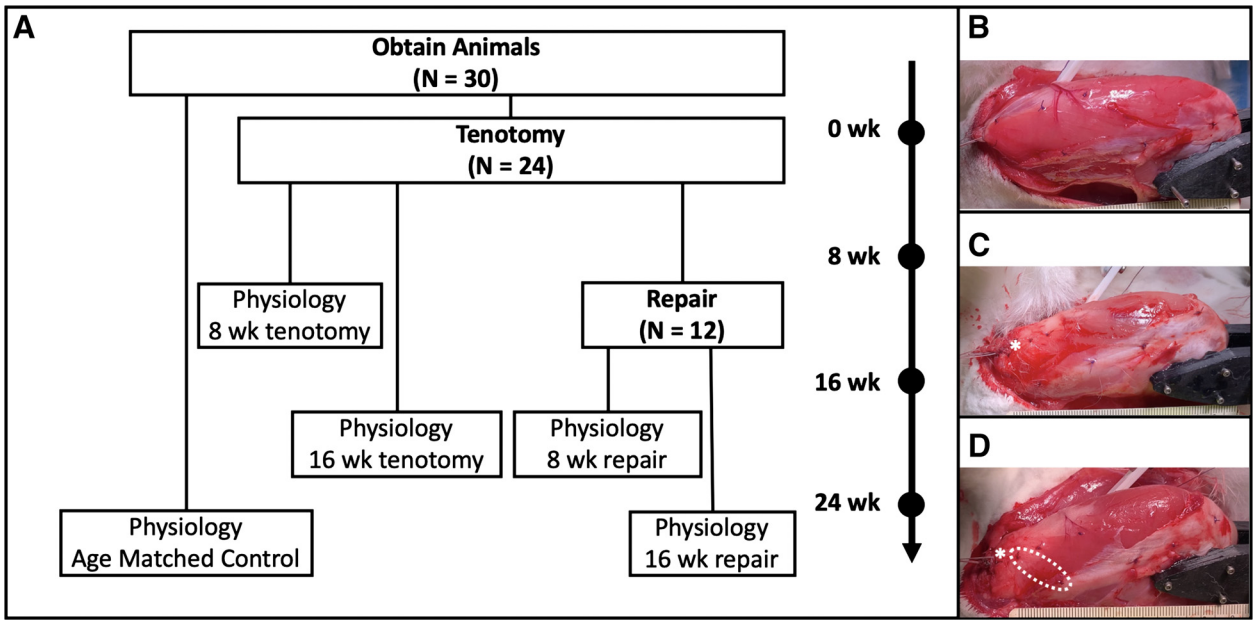

Figure 1. Experimental design. Timeline for generating each experimental group (*A*). Representative images during the physiology experiment for each experimental group (*B–D*). The age-matched control animals show healthy muscle tissue (*B*); tenotomy showing atrophy, fat accumulation, and muscle retraction at the myotendinous (MT) junction (*C*, MT junction indicated by *); and repair showing fat (*) and shortened muscle fibers (dotted region) at the myotendinous junction (*D*).

Isometric Length-Tension Protocol

The length-tension protocol was performed as previously described (29). Briefly, a series of 100 Hz tetanic contractions (pulse width: 0.3 ms; amplitude: 10 V) over a 640 ms period were delivered every 2 min. The first contraction was performed with the muscle set to its neutral length (the muscle length measured at 90° joint angle). For each subsequent contraction, the servomotor position was advanced 5 mm to lengthen the muscle. This was repeated until the muscle was operating on the descending limb of the length-tension curve, with a minimum of four contractions per animal.

Muscle and Fascicle Measurements

Suture markers were placed to define muscle and fascicle length, as done previously (29). Videos of each contraction were taken at 1080p resolution and 30 fps, and ImageJ software (31) was used to manually measure muscle and fascicle lengths and strains at rest and during the plateau region of each force-time record.

Muscle Architecture Measurements

After animals were euthanized, whole shoulders were fixed in 10% formalin in approximately the same orientation of 90° flexion to represent a neutral shoulder position. All architectural measurements were performed as previously described (11, 24, 29). The supraspinatus was exposed by removing the superficial muscles (trapezius and deltoid), and several fascicles were marked: three regions posterior and two regions anterior. Length and pennation angles of the marked fascicles were measured with digital calipers and a goniometer before carefully removing the supraspinatus from the scapula. The absolute values of pennation angles were then averaged to yield one measurement per muscle. Muscle mass was recorded from fixed muscles, and fascicles were removed from distinct regions and measured for raw fiber length (32, 33). Subsequent sarcomere length measurements were performed using laser diffraction, as previously described (34). Individual muscle fibers were dissected from fascicles and mounted on glass slides. Sarcomere length was recorded for three individual fibers and averaged for each fascicle. Sarcomere number was calculated by dividing fiber length by sarcomere length. Physiological cross-sectional area (PCSA) was calculated using the formula

$$\mathrm{PCSA} = \frac{\mathrm{mass}}{\rho \times L_{fn}} \cos\theta$$

where density was assumed to be 1.056 g/cm^3 (33), L_{fn} is the fiber length adjusted for sarcomere length, and θ is the average pennation angle for the muscle. Values averaged over all regions of the muscle are reported here, and individual regional data are included in the Supplemental Material (Supplemental Fig. S1; all Supplemental material is available at https://doi.org/10.6084/m9.figshare.13513539). One pair of shoulders for the 8 wk repair group was damaged during sample preparation and discarded.

Theoretical Length-Tension Curve

To incorporate the structural data with anticipated physiological effects, a length-tension curve was modeled for each experimental group using previously described methods (35). Briefly, a sarcomere level length-tension curve for rabbit skeletal muscle was generated: peak force was predicted at optimal sarcomere length (2.5 μm); the ascending limb started with minimum sarcomere length of 1.27 μm and the zone of single overlap beginning at 1.70 μm (67.59% maximum force); the descending limb spanned from optimal length to maximum sarcomere length of 4.02 μm. The model

was scaled from sarcomere to fiber level by multiplying sarcomere length values by serial sarcomere numbers. Then the model was scaled to the whole muscle level using architectural measurements from harvested supraspinatus muscles (Table 1). The following relationship was derived for determining the predicted muscle lengths

$$L_m = L_{mn} + L_f \cos\theta - L_{fn} \cos\theta$$

where L_m is the muscle length, L_{mn} is the optimal muscle length, L_f is the fiber length, L_{fn} is the optimal fiber length (determined from measured sarcomere length and raw fiber length), θ_n is the average pennation angle for each muscle as determined by the architectural analysis. The resting in vivo operating range for the SSP was determined using the intact muscle length-joint angle measurements, where the muscle length measured at max extension and max flexion sets the lower and upper physiological limits for the muscle length range. The activated in vivo operating range was defined by scaling the resting muscle lengths by the average muscle strain during contraction.

Data Analysis

Two-way ANOVA was used to compare architectural differences between experimental groups and between experimental and contralateral sides. Post hoc Sidak's test was used to compare groups, and Fisher's least significant difference (LSD) test was used to compare experimental versus contralateral side differences. Muscle strain, isometric tension, and isometric stress were analyzed using one-way ANOVA to compare the main effect of intervention and with post hoc Tukey's test for between-group comparisons. Two-way ANOVA (experimental vs. predicted and intervention group) with post hoc Sidak's tests was used to compare full width at half maximum (FWHM), peak force, and optimal muscle length. Significance level was set at $P < 0.05$ for all tests, and data are presented as means ± SD.

RESULTS

Muscle Architectural Changes

Supraspinatus muscle mass was significantly decreased in every intervention group (8 and 16 wk tenotomy, and 8 and 16 wk repair) compared with the unoperated side (P = 0.0043, $P < 0.0001$, P = 0.0017, and P = 0.0005, respectively). Both the 8 and 16 wk tenotomy groups had significantly decreased muscle mass compared with control animals, whereas neither of the repair groups was significantly lower than controls (Fig. 2A). Raw muscle length was significantly shorter after both 8 and 16 wk tenotomy, and 8 wk repair (Fig. 2B), increasing slightly from 9% shorter in the 8 wk tenotomy group to 4% shorter at 8 wk after repair. Muscle length after 16 wk repair was not significantly different between experimental and contralateral sides. There were no significant differences compared with age-matched controls. Raw fiber length decreased across all intervention groups compared with the contralateral side and age-matched controls (Fig. 2C), except the 8 wk tenotomy group showed no difference from age-matched controls. However, the 8 wk tenotomy group had significantly longer fibers than 8 wk repair (P = 0.0256).

Mean sarcomere length significantly increased to 2.40 μm at 8 wk after repair compared with 2.14 μm (age-matched controls) and 2.18 (16 wk repair), as well as compared with 2.20 μm on the contralateral side (P = 0.0076, P = 0.0211, and P = 0.0054, respectively) (Fig. 2D). At the same timepoint, mean sarcomere number was 9,864, significantly lower than both age-matched controls (12,219), 8 wk tenotomy (11,788), and its contralateral side (12,156) (P = 0.0119, P = 0.013, and $P < 0.0001$, respectively) (Fig. 2E). After 16 wk of tenotomy, serial sarcomere number decreased compared with its contralateral side, despite sarcomere length remaining unchanged, indicative of serial sarcomere deletion (Fig. 2, D and E). The normalized fiber length remained shorter than the contralateral side only for the 8 wk repair group (P = 0.0003), and it was also significantly shorter than both age-matched controls and 8 wk tenotomy (P = 0.0119 and P = 0.0131, respectively) (Fig. 2F).

Pennation angle showed the most differences between experimental conditions. All intervention groups showed significantly higher angles than the contralateral side (Fig. 2G), with the largest mean pennation angle of 36.56° at 8 wk post-repair compared with 22.23 in control animals, a difference of 40%. Only the 8 wk tenotomy group did not show a significant increase compared with age-matched controls. Both 8 and 16 wk tenotomy had a significantly lower mean pennation angle than 8 wk repair, but there was no difference in angles between 8 and 16 wk repair.

Finally, the calculated physiological cross-sectional area was 29% lower at 8 wk after tenotomy compared with age-matched controls (P = 0.0056). Both 8 and 16 wk tenotomy and 16 wk repair had a lower PCSA than the contralateral side (P = 0.0005, $P < 0.0001$, and P = 0.0085, respectively) (Fig. 2H).

Table 1. *Model parameters and values used for the predicted L-T curves*

	Control	8 wk Ten	16 wk Ten	8 wk Rep	16 wk Rep
Muscle length, mm	80.71	74.79	77.27	75.78	79.45
Sarcomere number (#)	12,219	11,788	10,814	9,864	10,721
Pennation angle, °	22.23	28.73	29.4	36.56	30.2
PCSA, cm^2	3.86	2.77	3.09	3.6	3.46

PCSA, physiological cross-sectional area; Rep, repair; Ten, tenotomy.

Peak Isometric Force and Stress

After tenotomy, peak isometric force was decreased by 22.4% after 8 wk (P = 0.17) and significantly decreased by 33.7% after 16 wk (P = 0.016) compared with the control group (69.5 ± 12.3 and 59.6 ± 19.7 vs. 89.4 ± 5.40 N, respectively) (Fig. 3A). Peak force was not significantly different between 8 and 16 wk tenotomy (P = 0.78). After repair, the 8 wk group tends to generate less force than controls (67.0 ± 19.0 N, P = 0.11). Although the 16 wk group was not significantly different than controls, mean peak force was decreased by 22.2% (69.7 ± 10.5 N, P = 0.18). Peak force was not significantly different between 8 and 16 wk repair (P = 0.99). In addition, peak force was not significantly improved after repair compared with either tenotomy group (Fig. 3A). Muscle stress (Fig. 3B) was not significantly different

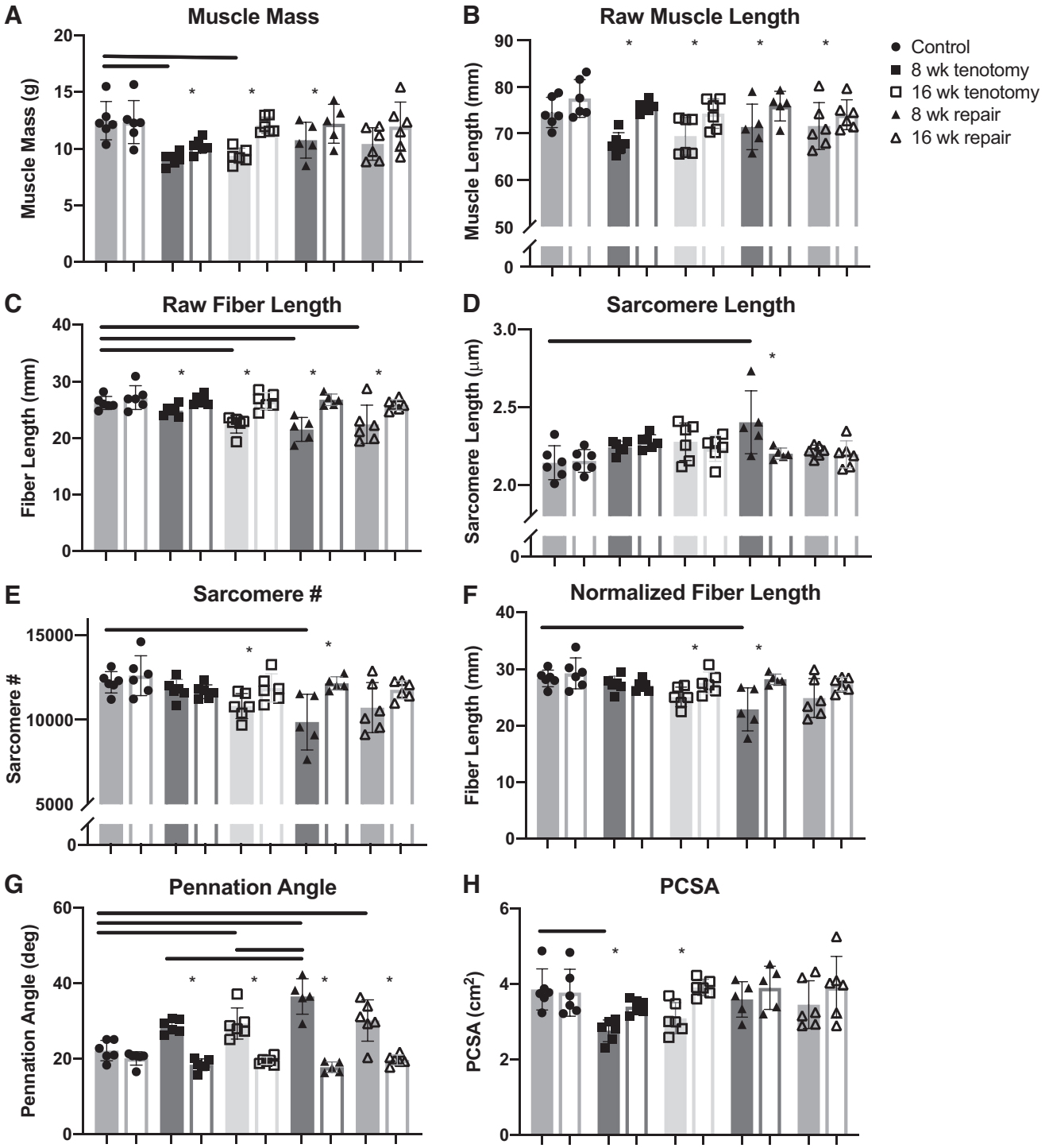

Figure 2. Architectural changes following tenotomy and repair. Average mass and raw muscle length (*A* and *B*), raw fiber length and sarcomere length (*C* and *D*), sarcomere number and normalized fiber length (*E* and *F*), pennation angle and PCSA (*G* and *H*) for rabbit SSP shown for each group. The experimental side (filled bars) and contralateral internal control (open bars) are shown (n = 6/group for control, 8 wk tenotomy, 16 wk tenotomy, and 16 wk repair; n = 5 for 8 wk repair). Bars indicate means ± SD. Data were analyzed with two-way ANOVA ($P < 0.05$), using post hoc Sidak's test to compare intervention groups (significance indicated by horizontal bars) and Fisher's LSD test to compare contralateral vs. experimental side differences (significance indicated by asterisks). LSD, least significant difference; PCSA, physiological cross-sectional area; SSP, supraspinatus.

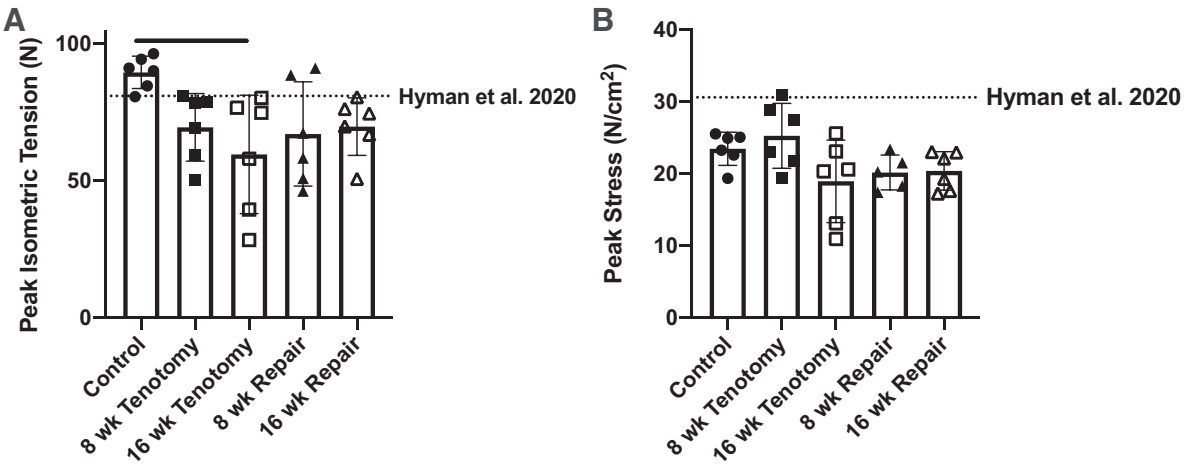

Figure 3. Peak isometric force (*A*) and stress (*B*) per animal (n = 30, n = 6 rabbits/group except 8 wk repair peak stress, which has n = 5). Dotted line shows values from previously published study on 6-mo-old NZ white rabbit SSP (29). Peak isometric force is significantly decreased after 16 wk tenotomy compared with controls. Each point represents one animal, and bars are shown as means ± SD. Data were analyzed with one-way ANOVA and post hoc Tukey's test ($P < 0.05$). Significance is indicated by horizontal bars. SSP, supraspinatus.

between groups, although there were two animals in the 16 wk tenotomy group with very low peak stress (~11 N/cm^2).

Muscle Strain

The measured whole muscle strain during each contraction was averaged for each animal (Fig. 4). The control group had significantly higher muscle strain than the 8 wk tenotomy, and 8 and 16 wk repair groups (7.86%, 4.06%, 4.54%, and 6.07%, respectively). Although not statistically significant, the whole muscle strain for 16 wk tenotomy (6.81%) decreased by 13% (P = 0.65). Muscle strain was significantly increased from 8 to 16 wk tenotomy ($P < 0.0001$), and 8 wk tenotomy compared with 16 wk repair (P = 0.0013). Eight week repair was significantly lower than both the 16 wk tenotomy and 16 wk repair groups (P = 0.008 and 0.006, respectively).

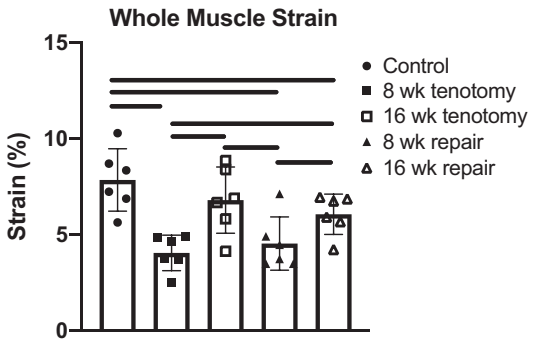

Figure 4. Whole muscle strain per animal (n = 30, n = 6 rabbits/group). Compared with controls, muscle strain was significantly lower after 8 wk tenotomy, 8 wk repair, and 16 wk repair. Eight week tenotomy was significantly lower than 16 wk tenotomy and 16 wk repair. Sixteen week tenotomy was significantly higher than 8 wk repair; 8 wk repair was significantly lower than 16 wk repair. Significance shown with horizontal lines. Each point represents one animal, and bars are shown as means ± SD. Data were analyzed with one-way ANOVA and post hoc Tukey's test ($P < 0.05$). Significance is indicated by horizontal bars.

Predicted L-T Curves

The predicted curves (Fig. 5) were generated for each group from the architecture data from each group (Table 1). The predicted curves varied in location (muscle length that yields peak isometric tension), width (muscle excursion dictated by fiber length), and height (peak isometric tension) based on the observed architectural changes. The predicted curves were statistically compared using three parameters: curve width [described by full width at half max (FWHM)], curve height (described by peak isometric force), and the length of peak

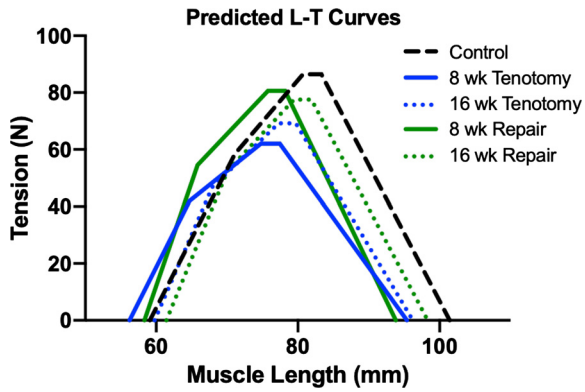

Figure 5. Predicted length-tension curves for each experimental group. After 8 wk tenotomy, the curve is shifted left, wider, and peak tension is lower than the control group. After 16 wk tenotomy, the curve is narrower and taller than 8 wk tenotomy but still has a lower predicted peak force than control. After 8 wk repair, the curve is similar in width and position to 8 wk tenotomy, with increased peak tension. Comparing 16 wk repair to 8 wk repair, the curve is shifted right due to increased muscle length, narrower due to decrease in pennation angle, and peak is similar due to unchanged PCSA. The predicted curve for 16 wk repair is visually most similar to the control curve. The predicted curves were statistically compared using three parameters: curve width [described by full width at half max (FWHM)], curve height (described by peak isometric force), and the length of peak force (described by optimal muscle length) with a one-way ANOVA and post hoc Tukey's test. No significant differences were noted in these theoretical comparisons. PCSA, physiological cross-sectional area.

force (described by optimal muscle length) with a one-way ANOVA and post hoc Tukey's test. No significant differences were noted in these theoretical comparisons.

Experimental Physiology

Experimental whole muscle length-tension curves were approximated as inverted parabolas (Fig. 6). Activated muscle length was used in these curves, as it more accurately describes the length-tension behavior of the SSP than resting muscle length (29). The control and 8 wk tenotomy animals (Fig. 6, *A* and *B*) most closely match the ascending limb and plateau of the predicted curve. Sixteen week tenotomy (Fig. 6*C*) is shifted left from the predicted curve; 8 wk repair (Fig. 6*D*) was the most disordered group studied. Sixteen week repair (Fig. 6*E*) is shifted right compared with the predicted curve, but the peak force is aligned with the prediction.

The experimental and predicted curves were statistically compared using three parameters: curve width (described by FWHM), curve height (described by peak isometric force), and the length of peak force (described by optimal muscle length) with a one-way ANOVA and post hoc Sidak's test. FWHM (Supplemental Table S1) was significantly different between the experimental and predicted curves for each group except for 8 wk repair ($P = 0.4125$). There were no significant differences between experimental and predicted curve height (Supplemental Table S2) or optimal muscle length (Supplemental Table S3) for any group.

DISCUSSION

The purpose of this study was to determine the structural and physiological consequences of rotator cuff tear and surgical repair over time through measuring muscle architecture and the length-tension relationship. Our hypotheses that architectural changes would demonstrate radial and longitudinal atrophy after tear and persist through repair, and that peak force would be decreased after tenotomy and repair, were supported. Surprisingly, muscle strain was lower after 8 wk tenotomy and repair, and similar to normal at 16 wk tenotomy and repair, refuting our initial hypothesis. Perhaps most importantly, our hypothesis that length-tension curves would be narrower and lower in magnitude after tenotomy and repair, based on structural changes in the muscles, was supported only after 16 wk repair. The remaining timepoint largely demonstrated an uncoupling between sarcomere organization (architecture) and physiology.

The architectural consequences of tenotomy indicate that muscle retraction and prolonged mechanical unloading lead to serial sarcomere loss, consistent with prior literature (12, 19). Despite the shorter fibers, the increased pennation angle seemed to overall maintain the width of the length-tension curve, which is consistent with Gerber et al.'s hypothesis that pennation angle increase is a compensatory mechanism to increase the force output and muscle excursion in the shortened, atrophied muscle (22). By 16 wk after tenotomy (Fig. 2), there is significant muscle loss, indicating sarcomere loss both in parallel (by muscle mass and PCSA decrease) and in series (by sarcomere number decrease).

After repair, sarcomere lengths are dramatically lengthened at 8 wk, indicating that the serial sarcomere loss persists in the initial stage after repair. The increased pennation angle at 8 wk suggests a lengthening of the tendon (as opposed to muscle) to reattach the muscle-tendon unit to the footprint. By 16 wk, some muscle length is recovered, as

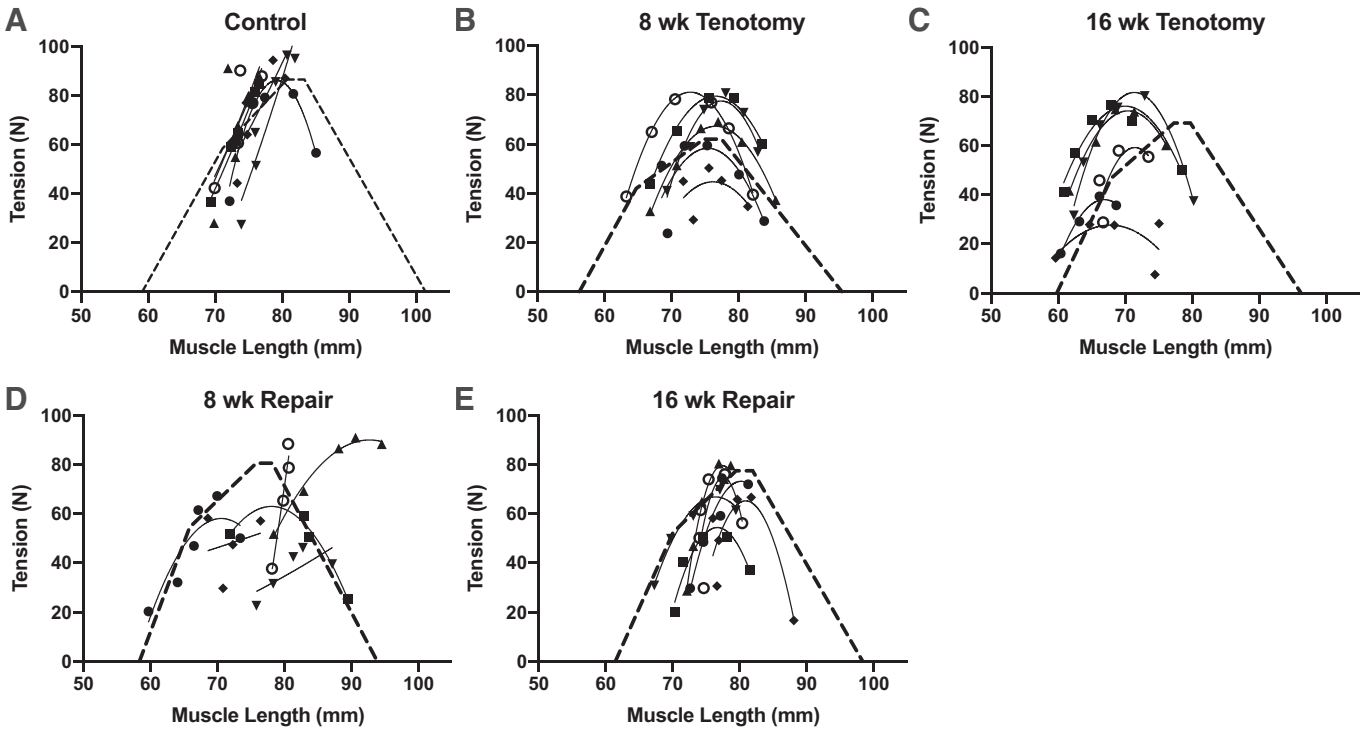

Figure 6. Predicted length-tension curves (dashed line) and individual data points fitted with second-order polynomial regressions for each rabbit in each experimental group (*A*–*E*). Each point represents one contraction with different symbols used for each animal ($n = 30$, $n = 6$ female rabbits/group).

well as sarcomere number and sarcomere length, indicating some functional recovery of the muscle.

Whole muscle strain is vastly different between experimental groups. After 8 wk of tenotomy, muscle strain is decreased by nearly 50%, which is not explained by structural changes (sarcomere length and sarcomere number are unchanged after 8 wk tenotomy compared with the contralateral side or control animals, Fig. 2). However, fibrosis is known to inhibit muscle strain and could be largely responsible for this decrease (20, 36). This appears to be similar after 8 wk of repair, which has been shown to induce an acute muscle injury itself, increasing muscle fibrosis (20). However, it is unlikely that this fibrosis predominates the physiological changes 8 wk postrepair. After 16 wk of either tenotomy or repair, muscle strain increases closer to the control animals. Many biological changes occurring to the muscle (fibrosis, muscle degeneration, fatty infiltration, etc.), which are not explored here, may be competing to influence muscle function (25–27).

Peak isometric tension was only significantly lowered after 16 wk of tenotomy and stress was not significantly different between any groups. However, we believe these are likely underpowered results, as there are large percentage changes (~20%–30%) between groups. A post hoc power analysis shows an $n = 12$ animals is required to detect statistical differences between these experimental groups. These data are consistent with our prior study in normal rabbits (29) but higher than previously reported by other groups in rabbit (15, 16). Despite larger animal masses used here, we believe the primary difference is due to the determination of optimal muscle length through twitch tensions rather than maximal tetanic contractions at multiple muscle lengths. This is due to the muscle shortening during contraction, leading the optimal muscle length to be longer at rest than the twitch tensions would suggest. Peak muscle stress in this study is slightly lower than our previous study in normal rabbit SSP, but within the range of normal literature.

Based on architectural parameters and the predicted muscle length equation, we analytically derived length-tension curves for each experimental group. Although the aponeurosis is not explicitly described in that equation, the equation implies that muscle length can be increased by fascicle length (serial addition of sarcomeres) or reductions in pennation angle. Increases in internal aponeurosis length would be captured by the pennation angle changes. Given the configuration of the SSP (multipennate with a long aponeurosis and a short external tendon), we believe that aponeurosis strains would be captured in this model (11, 22, 24). This is important as the aponeurosis likely undergoes physiologically relevant changes after tenotomy and repair.

The physiological consequences of tear and repair are seen in the experimental length-tension curves. The control animals are tightly clustered along the ascending limb and plateau of the length-tension curves. However, all of the intervention groups differ from their predicted curves in different ways (Fig. 6). After 8 wk tenotomy, the SSP primarily operating at the plateau and descending limbs of the length-tension curve (Fig. 6*B*), indicating a shortening of physiological operating range for the muscle. Curve height is highly variable for 8 wk tenotomy, 16 wk tenotomy, and 8 wk repair, but less variable in 16 wk repair. Optimal muscle length is fairly well predicted in 8 wk tenotomy, but not in 16 wk tenotomy or 8 wk repair. Curve width also matches the predicted curve for 8 wk tenotomy but not the other three intervention groups. This could be due to the varying levels of fiber shortening, muscle fibrosis (therefore stiffening), and fatty degeneration that are occurring in the muscles (19, 21, 35). Ultimately, the numerous changes occurring to the muscle after tenotomy (atrophy, degeneration, fibrosis, fatty infiltration, etc.) are dynamic processes which occur simultaneously, and they all contribute to physiological performance. From this study, we show that measures of PCSA are able to predict peak muscle force fairly well, which has high clinical value for estimating muscle function (5, 13, 16, 37).

This study has several limitations. First, there was higher than expected experimental variability between groups. Our methods allow for rigorous quality control of each force-time record, so we believe that this variability represents true physiological variability within and between groups. As such, although our samples sizes are consistent with other high-quality physiological experiments, statistical comparisons were marginally powered. This is a cautionary note to the field for two reasons, first physiological endpoints are unusual in the literature, but are arguably more important than histological endpoints, and second, a sample size of 6/group is on the large side relative to prior literature and could easily be double for more robust analyses. Another limitation is that we assume that our maximum recorded force is on the plateau of the length-tension curve for each rabbit, which could be off by the incremental unit length change in the muscle during the experiment. If this were true, we would expect errors in our prediction of optimal muscle length by up to 5 mm. In addition, our theoretical model utilizes averages to represent whole muscle architecture, rather than incorporating regional heterogeneity into account, which could impact model accuracy. And finally, the measurement of external and internal (aponeurosis) tendon strains may have shed more light onto the disparities between modeled and measured length tension curves. These measurements should be incorporated into future experiments.

In summary, this study provides a detailed picture of the structural and physiological changes that occur in the rabbit SSP after tenotomy and repair over time. We modeled a predicted length-tension curve based on animal-specific architecture data to reconcile structure with physiology. Through performing physiology testing, we assessed the length-tension relationship of each animal in each group, and we compare it with the predicted models. We report important physiological parameters, including the muscle strain, peak force, and peak stress for each group. These findings indicate persistent structural changes (both radial and longitudinal atrophy) and physiological deficiencies (decreased peak force and uncoupling of structure-function relationships) after tenotomy that do not significantly recover after repair. This work will allow researchers to better assess functional aspects of potential therapies for RC tear (5, 13, 16, 37).

SUPPLEMENTAL DATA

Supplemental Fig. S1 and Supplemental Tables S1–S3: https://doi.org/10.6084/m9.figshare.13513539.

GRANTS

The project described was partially supported by National Institutes of Health Grant R21AR072523.

DISCLOSURES

No conflicts of interest, financial or otherwise, are declared by the authors.

AUTHOR CONTRIBUTIONS

S.A.H. and S.R.W. conceived and designed research; S.A.H., I.T.W., L.S.V.-B., M.B.N., M.C.E., S.N.B., S.N.D., I.R., D.C.F., J.G.L., and A.S. performed experiments; S.A.H. and I.R. analyzed data; S.A.H. and S.R.W. interpreted results of experiments; S.A.H. prepared figures; S.A.H. and S.R.W. drafted manuscript; S.A.H., I.T.W., and S.R.W. edited and revised manuscript; S.A.H., I.T.W., L.S.V.-B., M.B.N., M.C.E., S.N.B., S.N.D., I.R., D.C.F., J.G.L., A.S., and S.R.W. approved final version of manuscript.

REFERENCES

1. **Collin P**, **Thomazeau H**, **Walch G**, **Gerber C**, **Mansat P**, **Favard L**, **Colmar M**, **Kempf JF**, **Hervé A**, **Betz M.** Clinical and structural outcome twenty years after repair of isolated supraspinatus tendon tears. *J Shoulder Elbow Surg* 28: 196–202, 2019. doi:10.1016/j.jse.2018.07.023.
2. **Goutallier D**, **Postel JM**, **Gleyze P**, **Leguilloux P**, **Van Driessche S.** Influence of cuff muscle fatty degeneration on anatomic and functional outcomes after simple suture of full-thickness tears. *J Shoulder Elbow Surg* 12: 550–554, 2003. doi:10.1016/s1058-2746(03)00211-8.
3. **Gerber C**, **Meyer DC**, **Schneeberger AG**, **Hoppeler H**, **von Rechenberg B.** Effect of tendon release and delayed repair on the structure of the muscles of the rotator cuff: an experimental study in sheep. *J Bone Joint Surg Am* 86: 1973–1982, 2004. doi:10.2106/00004623-200409000-00016.
4. **Gladstone JN**, **Bishop JY**, **Lo IKY**, **Flatow EL.** Fatty infiltration and atrophy of the rotator cuff do not improve after rotator cuff repair and correlate with poor functional outcome. *Am J Sports Med* 35: 719–728, 2007. doi:10.1177/0363546506297539.
5. **Hersche O**, **Gerber C.** Passive tension in the supraspinatus musculotendinous unit after long-standing rupture of its tendon: a preliminary report. *J Shoulder Elbow Surg* 7: 393–396, 1998. doi:10.1016/S1058-2746(98)90030-1.
6. **Petersen SA**, **Murphy TP.** The timing of rotator cuff repair for the restoration of function. *J Shoulder Elbow Surg* 20: 62–68, 2011. doi:10.1016/j.jse.2010.04.045.
7. **Shen PH**, **Lien SB**, **Shen HC**, **Lee CH**, **Wu SS**, **Lin LC.** Long-term functional outcomes after repair of rotator cuff tears correlated with atrophy of the supraspinatus muscles on magnetic resonance images. *J Shoulder Elbow Surg* 17: 1S–7S, 2008.doi:10.1016/j.jse.2007.04.014.
8. **Feeley BT**, **Liu M**, **Ma CB**, **Agha O**, **Aung M**, **Lee C**, **Liu X.** Human rotator cuff tears have an endogenous, inducible stem cell source capable of improving muscle quality and function after rotator cuff repair. *AM J Sports Med* 48: 2660–2668, 2020. doi:10.1177/0363546520935855.
9. **Gerber C**, **Meyer DC**, **Nuss KM**, **Farshad M.** Anabolic steroids reduce muscle damage caused by rotator cuff tendon release in an experimental study in rabbits. *J Bone Joint Surg Am* 93: 2189–2195, 2011. doi:10.2106/JBJS.J.01589.
10. **Wilde JM**, **Gumucio JP**, **Grekin JA**, **Sarver DC**, **Noah AC**, **Ruehlmann DG**, **Davis ME**, **Bedi A**, **Mendias CL.** Inhibition of p38 mitogen-activated protein kinase signaling reduces fibrosis and lipid accumulation after rotator cuff repair. *J Shoulder Elbow Surg* 25: 1501–1508, 2016.doi:10.1016/j.jse.2016.01.035.
11. **Gibbons MC**, **Sato EJ**, **Bachasson D**, **Cheng T**, **Azimi H**, **Schenk S**, **Engler AJ**, **Singh A**, **Ward SR.** Muscle architectural changes after massive human rotator cuff tear. *J Orthop Res* 34: 2089–2095, 2016. doi:10.1002/jor.23256.
12. **Tomioka T**, **Minagawa H**, **Kijima H**, **Yamamoto N**, **Abe H**, **Maesani M**, **Kikuchi K**, **Abe H**, **Shimada Y**, **Itoi E.** Sarcomere length of torn rotator cuff muscle. *J Shoulder Elbow Surg* 18: 955–959, 2009. doi:10.1016/j.jse.2009.03.009.
13. **Gerber C**, **Schneeberger AG**, **Hoppeler H**, **Meyer DC.** Correlation of atrophy and fatty infiltration on strength and integrity of rotator cuff repairs: a study in thirteen patients. *J Shoulder Elbow Surg* 16: 691–696, 2007. doi:10.1016/j.jse.2007.02.122.
14. **Meyer DC**, **Gerber C**, **Von Rechenberg B**, **Wirth SH**, **Farshad M.** Amplitude and strength of muscle contraction are reduced in experimental tears of the rotator cuff. *Am J Sports Med* 39: 1456–1461, 2011. doi:10.1177/0363546510396305.
15. **Fabiś J**, **Kordek P**, **Bogucki A**, **Mazanowska-Gajdowicz J.** Function of the rabbit supraspinatus muscle after large detachment of its tendon: 6-week, 3-month, and 6-month observation. *J Shoulder Elbow Surg* 9: 211–216, 2000.
16. **Valencia AP**, **Lai JK**, **Iyer SR**, **Mistretta KL**, **Spangenburg EE**, **Davis DL**, **Lovering RM**, **Gilotra MN.** Fatty infiltration is a prognostic marker of muscle function after rotator cuff tear. *Am J Sports Med* 46: 2161–2169, 2018. doi:10.1177/0363546518769267.
17. **Lieber RL.** *Skeletal Muscle Structure, Function, and Plasticity*. Wolters Kluwer Health Adis (ESP), 2011.
18. **Davis ME**, **Stafford PL**, **Jergenson MJ**, **Bedi A**, **Mendias CL.** Muscle fibers are injured at the time of acute and chronic rotator cuff repair. *Clin Orthop Relat Res* 473: 226–232, 2015. doi:10.1007/s11999-014-3860-y.
19. **Gibbons MC**, **Singh A**, **Anakwenze O**, **Cheng T**, **Pomerantz M**, **Schenk S**, **Engler AJ**, **Ward SR.** Histological evidence of muscle degeneration in advanced human rotator cuff disease. *J Bone Joint Surg Am* 99: 190–199, 2017. doi:10.2106/jbjs.16.00335.
20. **Mendias CL**, **Roche SM**, **Harning JA**, **Davis ME**, **Lynch EB**, **Sibilsky Enselman ER**, **Jacobson JA**, **Claflin DR**, **Calve S**, **Bedi A.** Reduced muscle fiber force production and disrupted myofibril architecture in patients with chronic rotator cuff tears. *J Shoulder Elbow Surg* 24: 111–119, 2015. doi:10.1016/j.jse.2014.06.037.
21. **Lieber RL**, **Fridén J.** Functional and clinical significance of skeletal muscle architecture. *Muscle Nerve* 23: 1647–1666, 2000. doi:10.1002/1097-4598(200011)23:11<1647::aid-mus1>3.0.co;2-m.
22. **Meyer DC**, **Hoppeler H**, **von Rechenberg B**, **Gerber C.** A pathomechanical concept explains muscle loss and fatty muscular changes following surgical tendon release. *J Orthop Res* 22: 1004–1007, 2004. doi:10.1016/j.orthres.2004.02.009.
23. **Sacks RD**, **Roy RR.** Architecture of the hind limb muscles of cats: functional significance. *J Morphol* 173: 185–195, 1982. doi:10.1002/jmor.1051730206.
24. **Ward SR**, **Hentzen ER**, **Smallwood LH**, **Eastlack RK**, **Burns KA**, **Fithian DC**, **Friden J**, **Lieber RL.** Rotator cuff muscle architecture: implications for glenohumeral stability. *Clin Orthop Relat Res* 448: 157–163, 2006. doi:10.1097/01.blo.0000194680.94882.d3.
25. **Farshad M**, **Meyer DC**, **Nuss KMR**, **Gerber C.** A modified rabbit model for rotator cuff tendon tears: functional, histological and radiological characteristics of the supraspinatus muscle. *Shoulder Elb* 4: 90–94, 2012. doi:10.1111/j.1758-5740.2011.00170.x.
26. **Matsumoto F**, **Uhthoff HK**, **Trudel G**, **Loehr JF.** Delayed tendon reattachment does not reverse atrophy and fat accumulation of the supraspinatus–an experimental study in rabbits. *J. Orthop. Res* 20: 357–363, 2002. doi:10.1016/S0736-0266(01)00093-6.
27. **Rubino LJ**, **Stills HF Jr**, **Sprott DC**, **Crosby LA.** Fatty infiltration of the torn rotator cuff worsens over time in a rabbit model. *Arthroscopy* 23: 717–722, 2007.doi:10.1016/j.arthro.2007.01.023.
28. **Uhthoff HK**, **Matsumoto F**, **Trudel G**, **Himori K.** Early reattachment does not reverse atrophy and fat accumulation of the supraspinatus–an experimental study in rabbits. *J Orthop Res* 21: 386–392, 2003. doi:10.1016/S0736-0266(02)00208-5.
29. **Hyman SA**, **Norman MB**, **Dorn SN**, **Bremner SN**, **Esparza MC**, **Lieber RL**, **Ward SR.** In vivo supraspinatus muscle contractility and architecture in rabbit. *J Appl Physiol (1985)* 129: 1405–1412, 2020. doi:10.1152/japplphysiol.00609.2020.
30. **McCracken TO**, **Kainer RA**, **Carlson , D.** Color Atlas of Small Animal Anatomy: The Essentials, Revised Edition (Online). Wiley-Blackwell. https://www.wiley.com/en-us/Color + Atlas + of + Small + Animal + Anatomy%3A + The + Essentials%2C + Revised + Edition-p-9780813816081 [2020 Aug 24].
31. **Schindelin J**, **Arganda-Carreras I**, **Frise E**, **Kaynig V**, **Longair M**, **Pietzsch T**, **Preibisch S**, **Rueden C**, **Saalfeld S**, **Schmid B**, **Tinevez J-Y**, **White DJ**, **Hartenstein V**, **Eliceiri K**, **Tomancak P**, **Cardona A.**

Fiji: an open-source platform for biological-image analysis. *Nat Methods* 9: 676–682, 2012. doi:10.1038/nmeth.2019.

32. **Mathewson MA**, **Kwan A**, **Eng CM**, **Lieber RL**, **Ward SR.** Comparison of rotator cuff muscle architecture between humans and other selected vertebrate species. *J Exp Biol* 217: 261–273, 2014. doi:10.1242/jeb.083923.
33. **Ward SR**, **Lieber RL.** Density and hydration of fresh and fixed human skeletal muscle. *J Biomech* 38: 2317–2320, 2005. doi:10.1016/j.jbiomech.2004.10.001.
34. **Lieber RL**, **Yeh Y**, **Baskin RJ.** Sarcomere length determination using laser diffraction. Effect of beam and fiber diameter. *Biophys J* 45: 1007–1016, 1984. doi:10.1016/S0006-3495(84)84246-0.
35. **Winters TM**, **Takahashi M**, **Lieber RL**, **Ward SR.** Whole muscle length-tension relationships are accurately modeled as scaled sarcomeres in rabbit hindlimb muscles. *J Biomech* 44: 109–115, 2011. doi:10.1016/j.jbiomech.2010.08.033.
36. **Gumucio JP**, **Davis ME**, **Bradley JR**, **Stafford PL**, **Schiffman CJ**, **Lynch EB**, **Claflin DR**, **Bedi A**, **Mendias CL.** Rotator cuff tear reduces muscle fiber specific force production and induces macrophage accumulation and autophagy. *J Orthop Res* 30: 1963–1970, 2012. doi:10.1002/jor.22168.
37. **Gerber C**, **Schneeberger AG**, **Beck M**, **Schlegel U.** Mechanical strength of repairs of the rotator cuff. *J Bone Joint Surg Br* 76: 371–380, 1994. doi:10.1302/0301-620X.76B3.8175836.